Journal of Membrane Science 634 (2021) 119393

Contents lists available at ScienceDirect

Journal of Membrane Science

journal homepage: www.elsevier.com/locate/memsci

Fabrication of *c*-oriented ultrathin TCPP-derived 2D MOF membrane for precise molecular sieving

Yifan Song [a], Yanwei Sun [a], Dongying Du [b], Mu Zhang [a], Yi Liu [a], Liangliang Liu [a], Taotao Ji [a], Gaohong He [a], Yi Liu [a,*]

[a] *State Key Laboratory of Fine Chemicals, School of Chemical Engineering, Dalian University of Technology, Linggong Road No. 2, Ganjingzi District, Dalian, 116024, China*

[b] *Institute of Functional Material Chemistry, Faculty of Chemistry, Northeast Normal University, 5268 Renmin Street, Changchun, 130024, China*

ARTICLE INFO

Keywords:
Gas separation
Metal-organic framework
Membranes
Nanosheets
Orientation

ABSTRACT

Two-dimensional (2D) membrane has brought promising opportunities to achieve the separation performance for overcoming the Robeson upper bound. Nevertheless, precise control of the in-plane pore size as well as the interlayer structure on a microscopic scale remains a great challenge. In this work, we produced well-intergrown, highly *c*-oriented ultrathin (ca. 80 nm-thick) 2D Cu-TCPP membranes on the porous alumina substrates through in-situ solvothermal method. Regular vertical stacking of single Cu-TCPP layers along the *c*-axis through van der Waals interactions resulted in narrowed pore size (equivalent to ~5.4 Å) and interlocked interlayer gallery. Gas permeation results indicated that prepared Cu-TCPP membranes showed precise size-selective molecular sieving behavior, owing to rational interlayer stacking on a microscopic scale as well as deliberate microstructural manipulation on a mesoscopic scale.

1. Introduction

Two-dimensional (2D) membrane has become a promising research topic for decades due to the hopeful prospects for overcoming Robeson upper bound line, relying on the minimized mass transfer barrier and diversified selective diffusion pathways (via in-plane pores or interlayer galleries) [1–4]. Nevertheless, there are still obstacles at different scales that must be conquered. On a microscopic scale, ideally both in-plane pores and interlayer galleries of 2D membranes should be highly uniform in terms of size and shape, which was the perquisite for precise molecular sieving [5–7]. On a mesoscopic scale, microstructure manipulation like the preferred orientation of 2D membrane has become indispensable to reduce the barrier layer thickness and non-selective defects along the preferred diffusion direction [8,9]. It was noted that common 2D membranes, including graphene oxides (GOs), 2D zeolites, 2D metal-organic frameworks (MOFs), transition metal dichalcogenides (TMDCs), 2D covalent-organic frameworks (COFs), and MXenes were generally prepared by first exfoliation of bulk layered precursors into uniformly dispersed nanosheets (NSs) and then reassembled on porous substrates via vacuum filtration [2,4], thermal dip-coating [1,8] or spin-coating [3]. Despite being very effective, it remained a great challenge to precisely control the shape, size, and uniformity of in-plane pores and interlayer structures on a microscopic scale as well as membrane microstructure on a mesoscopic scale. In addition, the manufacturing process was highly demanding in terms of expertise and experience.

2D MOF as a representative of 2D materials possessed highly uniform in-plane pores and interlayer galleries, making them excellent candidates for high performance separation membranes [10]. Nevertheless, owing to the immaturity of reticular chemistry at the current stage, it has remained a challenging task to precisely tune the shape and size of in-plane pores and interlayer galleries of 2D MOF membranes. For instance, tetrakis (4-carboxyphenyl) porphyrin (TCPP)-derived 2D MOF materials have shown fascinating properties in catalysis, optics, electronics, and biology due to the rich functionality of porphyrin and its derivatives [11]. Currently plenty of researches have been conducted on the fabrication of TCPP-derived 2D MOF thin films [12,13]. Nevertheless, to date there has been no reports on the fabrication of polycrystalline TCPP-derived 2D MOF membranes, even though they may exhibit superior separation performance relying on highly tailorable in-plane pores (including pore size and functionality) and interlayer structure (including stacking mode and interlayer spacing).

---

* Corresponding author.
E-mail address: diligenliu@dlut.edu.cn (Y. Liu).

https://doi.org/10.1016/j.memsci.2021.119393
Received 11 February 2021; Received in revised form 5 April 2021; Accepted 30 April 2021

As schematically illustrated in Fig. 1a, the in-plane pore size of single-layered TCPP-derived 2D MOF NSs was estimated to be ~10.4 Å which, however, remained too large for accurate discrimination of industrially important gas pairs with smaller kinetic diameters. Therefore, fine-tuning the equivalent in-plane pore size of TCPP-derived 2D MOF materials has become indispensable for realizing precise molecular sieving. Common methods, such as in-situ or post-synthetic functionalization of MOF membrane with ligands bearing bulky functional groups, may be valid for narrowing the pore size to a certain extent [14]; nevertheless, rational design and facile control over the size, shape, and uniformity of in-plane pores as well as interlayer galleries remained a great challenge.

The interlayer structure, in particular the stacking mode of single-layered 2D MOF NSs, often shows significant influence on gas separation behavior of 2D MOF membranes. Yang et al. for instance, prepared ultrathin 2D Zn_2 $(bIm)_4$ molecular sieve nanosheet membranes through the exfoliation of layered bulk counterparts by hot-drop coating. Gas permeation performance test indicated that elevating the temperature resulted in increased H_2 permeance and higher selectivity towards the H_2/CO_2 gas pair, which could be explained by the disorder stacking of 2D Zn_2 $(bIm)_4$ nanosheets facilitating sufficient exposure of in-plane pores [1]. In the case of TCPP-derived 2D MOF materials, previous studies indicated that the exact stacking sequence of the layers was strongly dependent on the type of central metal ions [11,15]. For instance, single-layered Cu-TCPP NSs adopted the AB stacking mode along the *c*-axis, with the B layers shifted from the vertical positions of the A layers by one-fourth of the unit cell along the *a*-axis [12,13,16]. As a result, the equivalent pore size of Cu-TCPP layered bulk crystals along the *c*-axis was reduced to ~5.4 Å, which held great promise for effective separation of small-sized gas molecules via precise sized-based molecular sieving. Simultaneously, the interlocked interlayer structure (2.7 Å), obtained by subtracting the size of carbon atom (1.8 Å), effectively precluded gas permeation through 2D Cu-TCPP membranes via any non-selective defects/interlayer galleries except for equivalent 5.4 Å-sized in-plane pores, which was quite beneficial for realizing high precision molecular sieving [16]. In addition, aiming at minimizing the non-selective grain boundary defects and shortening the gas diffusion path along the *c*-axis on a mesoscopic scale, it is highly desirable to fabricate well-intergrown, highly *c*-oriented ultrathin 2D Cu-TCPP membranes via a facile in-situ synthetic route, which may exhibit superiority over the exfoliation-reassembly method in terms of structural integrity and regularity of both in-plane pores and interlayer galleries besides process simplicity.

Based on the above concerns, herein we provided a facile in-situ solvothermal method to prepare 2D Cu-TCPP membranes with the desired microstructure on porous α-Al_2O_3 substrates (Fig. 1b). Briefly, prior to membrane fabrication, ZnO buffer layers derived from ZnAl–NO_3 layered double hydroxide (LDH) precursor membranes were deposited on porous substrates. Subsequently, LDH-based ZnO buffer layer-modified substrates were put in DMF precursor solutions containing cupric acetylacetonate (Cu(acac)$_2$), H_2TCPP, and triethylamine (TEA). Finally, in-situ solvothermal reaction was conducted under controlled conditions, thereby forming well-intergrown, highly *c*-oriented ultrathin 2D Cu-TCPP membranes. Among various synthetic parameters, substrate surface decoration with LDH-based ZnO buffer layers, employing Cu(acac)$_2$ as copper source, and addition of TEA additives in precursor solutions were found to be crucial in preparing 2D Cu-TCPP membranes with the desired microstructure. To the best of our knowledge, this work represented the study on fabricating polycrystalline TCPP-derived 2D MOF membranes for the first time.

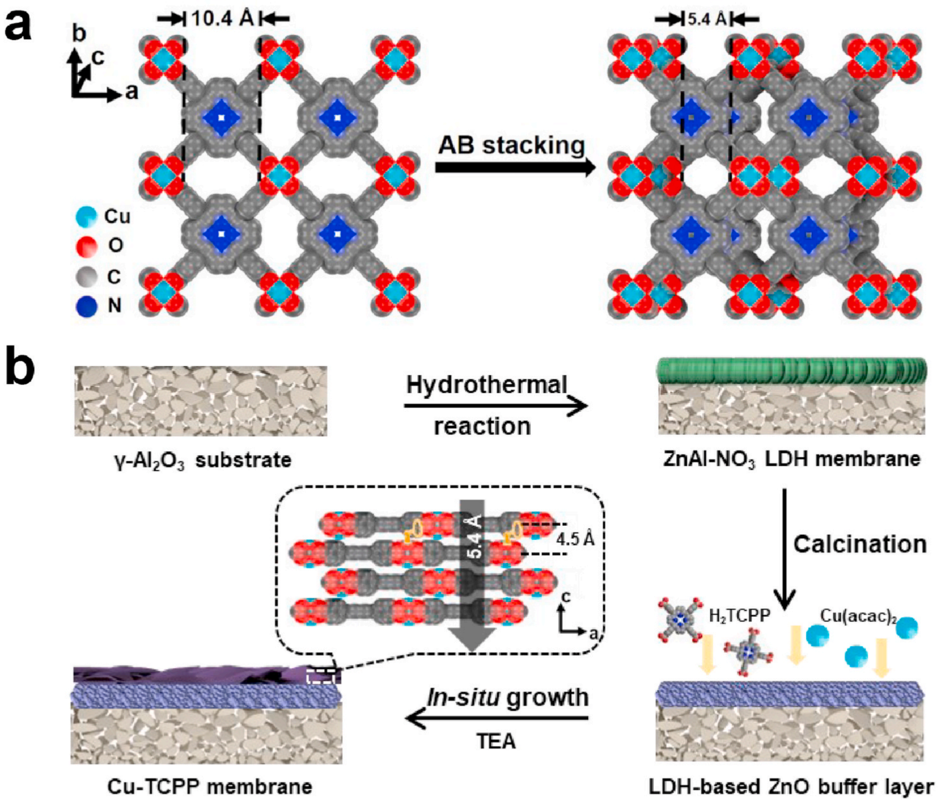

Fig. 1. (a) Schematic diagram of narrowed pore size of Cu-TCPP membrane in comparison with a single Cu-TCPP layer (Cu: light blue, C: grey, N: blue, O: red, H atoms are omitted). (b) Schematic illustration of preparing the well-intergrown, highly *c*-oriented ultrathin 2D Cu-TCPP membrane by in-situ solvothermal growth. (For interpretation of the references to colour in this figure legend, the reader is referred to the Web version of this article.)

2. Experimental section

2.1. Fabrication of gel-based ZnO buffer layer

Firstly, ZnO sol was obtained by adding 8.3 g $Zn(Ac)_2{\cdot}2H_2O$ to 48 ml EGME solution at 343 K with the help of fierce stirring. Then the solution was aged at 298 K for 10 h after slowly adding 2.4 ml MEA. Finally, the ZnO buffer layer was obtained by spin-coating for 60 s at 3000 rpm followed by calcination at 673 K for 2 h or simple drying at 343 K for 8 h.

2.2. Fabrication of LDH-based ZnO buffer layer

Firstly, we prepared ZnAl–NO_3 LDH membrane following the well-documented procedure [17]. Then prepared ZnAl–NO_3 LDH membrane was slowly calcined at 623 K for 9 h. Finally, calcined LDH membranes were slowly cooled to 298 K within 10 h.

2.3. Growth of randomly aligned Cu-TCPP membrane on gel-/LDH-based ZnO buffer layer

Firstly, the solution was obtained by adding 38 mg H_2TCPP to 15 ml DMF solution containing 25 mg $Cu(NO_3)_2{\cdot}3H_2O$ under vigorous stirring at room temperature. Then the buffer layer-modified substrate was put in a Teflon-lined stainless vessel. Finally, after being heated at 333 K for 6 h the membrane was removed from the vessel, and then washed with DMF and dried at 343 K.

2.4. Growth of vertically aligned Cu-TCPP membrane on LDH-based ZnO buffer layer

Firstly, the solution was obtained by adding 38 mg H_2TCPP to 15 ml DMF solution containing 25 mg $Cu(acac)_2$ under vigorous stirring at room temperature. Then the buffer layer-modified substrate was put in a Teflon-lined stainless vessel. Finally, after being heated at 333 K for 6 h the membrane was removed from the vessel, washed with DMF, and dried at 343 K.

2.5. Growth of the well-intergrown, highly c-oriented ultrathin Cu-TCPP membrane on LDH-based ZnO buffer layer

Firstly, the solution was obtained by adding 38 mg H_2TCPP to 15 ml DMF solution containing 150 mg TEA and 25 mg $Cu(acac)_2$ under vigorous stirring at room temperature. Then the buffer layer-modified substrate was put in a Teflon-lined stainless vessel. Finally, after being kept at 333 K for 6 h, the membrane was removed from the vessel, washed with DMF, and dried at 343 K.

2.6. Characterization

XRD results were obtained on Rigaku SmartLab diffractometer. FT-IR spectra were obtained on Bruker Equinox 55 spectrometer. Microstructure of the samples were investigated by the SEM (NOVA NanoSEM 450). The composition of near-surface elements was obtained from X-ray photoelectron spectroscopy (XPS).

2.7. Gas permeation performance test

We evaluated the gas separation performance as follow: Volumetric flow rate at the feed side was 50 ml min^{-1} and the permeated gas was removed by sweep gas. Mixed gas separation performance was tested by fixing the volumetric flow rate of each gas at 50 ml min^{-1}. In both cases, Ar was served as the sweep gas, the volumetric flow rate was controlled at 50 ml min^{-1}, and the pressure was maintained at 1 bar at the feed side. We employed Gas Chromatograph (GC7890T) to analyze the content of the permeated gases. Separation factor (SF) $\alpha_{i,j}$ was defined by equation in which $X_{i,perm}$ and $X_{j,perm}$ represented molar ratios of permeable components (*i*, *j*); $X_{i,feed}$ and $X_{j,feed}$ represented molar ratios of components (*i, j*) at feed side.

$$\alpha_{i/j} = \frac{X_{i,perm} / X_{j,perm}}{X_{i,feed} / X_{j,feed}}$$

3. Results and discussion

3.1. Substrate surface modification with LDH-based ZnO buffer layers

Initially, we tried depositing appropriate buffer layer on porous α-Al_2O_3 substrate. Indeed, the introduction of CuO buffer layer may provide the nucleation sites and serve as the Cu^{2+} source. Nevertheless, our experimental results indicated that this was not the case. The use of CuO buffer layer inevitably led to the low heterogeneous nucleation density and the loss of preferred orientation of 2D Cu-TCPP layer. Alternatively, we tried depositing smoother ZnO buffer layer with a facile sol-gel method (Fig. S1) [18,19]. Nonetheless, it remained impractical to warrant the membrane quality in terms of orientation (Fig. S2) or continuity (Fig. S3), which could be attributed to the low chemical activity of gel-based ZnO buffer layer during the formation of 2D Cu-TCPP membrane even under optimal reaction conditions [18,20,21]. Our previous research indicated that the ZnO buffer layer prepared by calcination of ZnAl–NO_3 LDH precursor membrane (Fig. S4) possessed much higher reactivity, owing to the high surface free energy and dangling bond density of 10 nm-sized ZnO nanocrystal building blocks (Fig. 3a, S5) [22,23]. Therefore, in this study, the ZnO buffer layer was prepared by calcination of ZnAl–NO_3 LDH precursor membrane instead of common sol-gel processing.

3.2. Fabrication of well-intergrown, c-oriented ultrathin 2D Cu-TCPP membranes

A recent study indicated that controlled exposure of atomic-layer-deposited (ALD) ZnO-coated PP fibers to $Cu(NO_3)_2$ and H_2TCPP led to the formation of highly *c*-oriented, though discrete and fragile, 2D Cu-TCPP thin films [24]. Nevertheless, our experimental results indicated that this was not the case. Substantial homogeneous nucleation was triggered in the bulk solution during the solvothermal process, yielding randomly aligned 2D Cu–TCPP membrane comprising severely aggregated platelet-shaped crystals on the substrate (Fig. 2a and b). EDXS pattern (Fig. S6) of randomly aligned Cu-TCPP membrane showed a clear boundary between the Cu-TCPP membrane and the LDH-based ZnO buffer layer. The large discrepancy in microstructure may be ascribed to different physicochemical properties and geometric shapes between ALD and LDH based-ZnO buffer layers [22]. Therefore, concurrent suppression of crystal nucleation in the bulk solution and modulation of crystal growth on the ZnO buffer layer surface were required to prepare 2D Cu-TCPP membrane with the desired microstructure.

It has been well recognized that in comparison with common inorganic metal sources, organic metal sources dissolved more slowly and homogenously in the organic precursor solution [25–27]. In this study, $Cu(acac)_2$ was used as copper source instead of $Cu(NO_3)_2$ with the purpose of retarding the excessive crystal nucleation in the bulk solution and therefore, alleviating random alignment of platelet-shaped Cu-TCPP crystals on the substrate during solvothermal process (Fig. 2c and d, S7). Moreover, a recent study reported by Zhang indicated that NH_4OH, a basic structural modulator, enabled effective promotion of the (002) crystal plane epitaxial growth of $[Zn_2(bIm)_4]$ nanosheets and eventually led to the formation of highly *c*-oriented 2D $[Zn_2(bIm)_4]$ molecular sieve nanosheet membrane [28]. Considering the structural similarity between Cu-TCPP and $[Zn_2(bIm)_4]$, herein we proposed to modulate Cu-TCPP crystal growth on the ZnO buffer layer via addition of basic amines in the precursor solution. Among various amines tested, the use of TEA was proven more effective for concurrent promotion of the

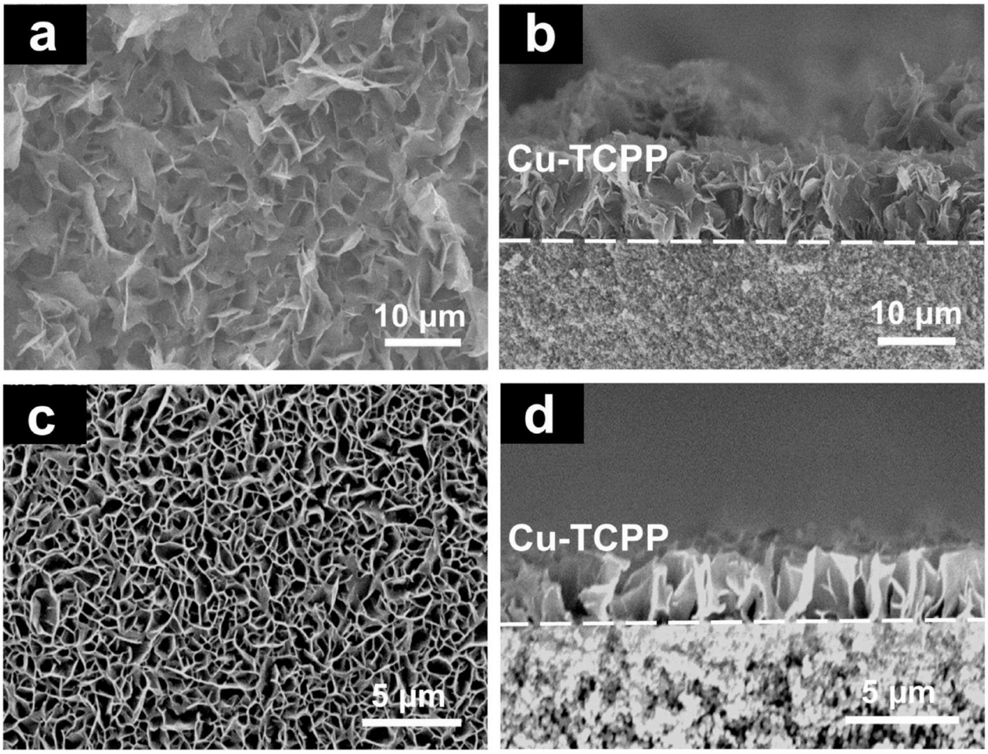

Fig. 2. Top and cross-sectional SEM images of Cu-TCPP membranes prepared on LDH-based ZnO buffer layers in the absence of TEA with (a, b) $Cu(NO_3)_2 \cdot 3H_2O$ and (c, d) $Cu(acac)_2$ metal sources, respectively.

in-plane growth and suppression of the undesired out-of-plane growth of 2D Cu-TCPP membrane (Fig. S8). Top and cross-sectional SEM images showed that prepared Cu-TCPP membrane was highly uniform, well-intergrown (Fig. 3b and c) and only 80 nm-thick (Fig. 3d). Cross-sectional EDX patterns (Fig. S9) showed a clear boundary between the 2D Cu-TCPP membrane and LDH-based ZnO buffer layer-modified substrate. FT-IR (Fig. 3f) and XPS spectra indicated the existence of $Cu_2(COO)_4$ paddle-wheel units (Fig. 3g–i), which was in agreement with Cu-based secondary building units of Cu-TCPP phase as reported in the literature [29]. FT-IR spectra of prepared Cu-TCPP membrane, as shown in Fig. 3f, showed absorption peaks around 1600 cm^{-1} and 1400 cm^{-1}, which could be assigned to the C=O asymmetric stretching vibration ($\nu_{asym}C = O$) and the C=O symmetric stretching vibration ($\nu_{sym}C = O$), respectively. The above results indicated the formation of coordination bonds between Cu-based secondary building units and carboxyl groups of the H_2TCPP ligands. Moreover, as shown in the XPS spectra (Fig. 3h), the C 1s peaks at 285 eV and 288.8 eV corresponded to the C–C and C=O bonds in the 2D Cu-TCPP structure, while the Cu 2p spectra showed two characteristic peaks at 933.2 eV and 935.2 eV, which could be assigned to the Cu $2p_{3/2}$ spin-orbit state, thereby confirming the presence of Cu^{2+} in 2D Cu-TCPP nanosheets (Fig. 3i). AFM measurements showed the thickness of Cu-TCPP nanosheets reached ~13.0 nm (equivalent to ~29 single Cu-TCPP layers, shown in Fig. S10). Moreover, the XRD pattern of obtained Cu-TCPP membrane indicated a clear diffraction peak at 2θ value of 19.3° corresponding to the (002) crystal plane, which connivingly demonstrated that prepared 2D Cu-TCPP membrane was dominantly *c*-oriented (Fig. 3e) [16,24]. Relatively weak intensity of (002) diffraction peak of prepared Cu-TCPP membrane could be attributed to the ultrathin layer thickness of prepared Cu-TCPP membrane (ca. 80 nm-thick, equivalent to ~7 single Cu-TCPP nanosheets) [30,31].

3.3. *Gas separation performance of 2D Cu-TCPP membranes*

Herein, both single and mixed gas permeation tests were performed on prepared highly *c*-oriented ultrathin 2D Cu-TCPP membrane. Our experimental results indicated that single gas permeance through the prepared *c*-oriented ultrathin 2D Cu-TCPP membrane decreased steadily as the kinetic diameters of permeating molecules increased and the ideal gas selectivity of H_2/CO_2, H_2/N_2, H_2/CH_4 and H_2/SF_6 gas pairs achieved 8.7, 40.2, 56.0 and 236.5, respectively (shown in Fig. 4a, S11). Particularly it was noted that the permeance of SF_6 (1.12×10^{-9} mol m^{-2} $s^{-1} \cdot Pa^{-1}$) was about four times lower than that of CH_4 (4.77×10^{-9} mol m^{-2} $s^{-1} \cdot Pa^{-1}$), which coincided well with the fact that equivalent in-plane pore size of 2D Cu-TCPP membrane fell between CH_4 (3.8 Å) and SF_6 (5.5 Å).

Compared with other pristine polycrystalline MOF membranes, prepared 2D Cu-TCPP MOF membrane exhibited superior separation performance towards H_2/N_2, H_2/CH_4, and H_2/SF_6 except for very few 2D MOF membranes with pore apertures smaller than 3.0 Å, i.e., $[Zn_2(bIm)_4]$ (2.6 Å), $[Zn_2(bIm)_3]$ (2.6 Å), and MAMS-1 (2.9 Å) which were intrinsically more H_2-selective (Fig. 4b, S12 and Table S1) [8–10,14,18,32–44]. It was noticed that, although both H_2/N_2 and H_2/CH_4 selectivity of 2D 40 nm-thick MAMS-1 and 200 nm-thick Zn_2 $(bIm)_4$ membranes was higher than 2D Cu-TCPP membrane, H_2 permeance of the 2D Cu-TCPP membrane was remarkably higher than the two aforementioned membranes. In addition, as shown in Table S2, compared with most 2D membranes, prepared 2D Cu-TCPP membrane still exhibited higher selectivity towards H_2/N_2 and H_2/CH_4 gas pairs. For instance, although H_2 permeance of graphene-based, TMDC and MXene membranes were higher than that of 2D Cu-TCPP membrane, the H_2/N_2 and H_2/CH_4 selectivity of 2D Cu-TCPP membrane remained higher than the aforementioned membranes. Furthermore, as shown in Table S3, compared with other types of zeolite or MOF membranes with pore size around 5.4 Å including MFI zeolite, UiO-66 series, and NH_2-MIL-125(Ti) membranes, prepared Cu-TCPP membrane exhibited comparable H_2 permeance but widely varying H_2 permeability, which may result from the following factors: 1) On a microscope scale, it is well known that multiple diffusion pathways in membranes may contribute to enhanced gas permeation [8,45]. It is noticed that there are multiple diffusion pathways including interconnected pore channels and cages

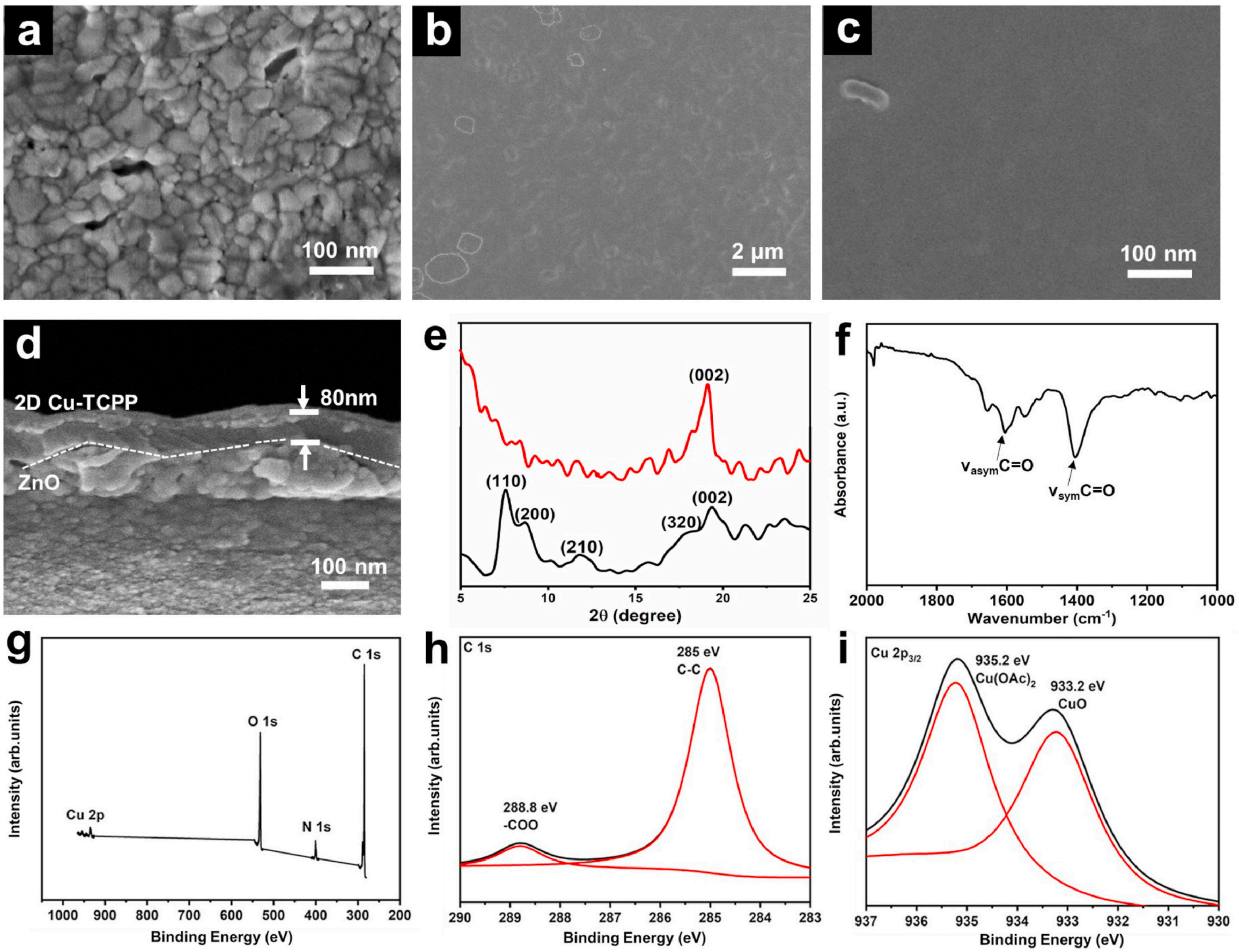

Fig. 3. SEM images of (a) LDH-based ZnO buffer layer, (b, c, d) 2D Cu-TCPP membrane obtained by in-situ solvothermal growth. (e) XRD patterns of Cu-TCPP powders (black line) and prepared 2D Cu-TCPP membrane (red line). (f) FT-IR and (g, h, i) XPS spectra of prepared 2D Cu-TCPP membrane. (For interpretation of the references to colour in this figure legend, the reader is referred to the Web version of this article.)

accessible for gas permeation through the above membranes. In contrast, gas molecules are only allowed to permeate through the 2D Cu-TCPP membrane via 5.4 Å-sized one-dimensional straight channels, potentially leading to varying diffusion barrier. 2) On a mesoscopic scale, the microstructure of zeolite or MOF membranes (like preferred orientation, thickness, grain size, and grain boundary structure) often exerts significant influence on their separation performances, e.g., UiO-66 series membranes [27,33,46,47]. 3) On a macroscopic scale, the barrier property of the support may greatly affect gas permeabilities of zeolite or MOF membranes.

It is well recognized that the membrane selectivity ($S_{mem(i/j)}$) can be well described by the interplay of adsorption selectivity ($S_{ads(i/j)}$) and diffusion selectivity ($S_{diff(i/j)}$) according to the following equation: $S_{mem(i/j)} = S_{ads(i/j)} \times S_{diff(i/j)}$ [48]. On the one hand, since there is no significant difference in adsorption interaction with the 2D TCPP framework for both non-polar molecules H_2 and CH_4, prepared 2D TCPP membrane should exhibit low adsorption selectivity, i.e., $S_{ads(H2/CH4)} \approx 1$ [24]; on the other hand, since the kinetic diameter of H_2 (2.9 Å) is smaller than that of CH_4 (3.8 Å), the diffusion coefficient of H_2 in the 2D TCPP framework should be remarkably higher than CH_4, thereby leading to higher $S_{diff(H2/CH4)}$ ($\gg 1$). As a result, the H_2/CH_4 selectivity, i.e., $S_{mem(H2/CH4)}$, is comparatively high (~60). Obviously, effective intergrowth, orientation, and thickness control cooperatively contributed to the precise molecular sieving ability of prepared 2D Cu-TCPP membrane.

The influence of operating temperature on gas separation performance of prepared 2D Cu-TCPP membrane was investigated further. Our experimental results indicated that both separation factor of equimolar H_2/CH_4 (Fig. 4c) and H_2/SF_6 (Fig. 4e) gas pairs steadily increased accompanying increases in operating temperature from 303 K to 453 K. Moreover, H_2 permeance increased with the operating temperature either, which could be attributed to a gradual pronounced molecular sieving effect [1,9]. Furthermore, prepared 2D Cu-TCPP membrane showed impressive long-term stability. It was observed that both separation factor of equimolar H_2/CH_4 (Fig. 4d) and H_2/SF_6 (Fig. 4f) gas pairs remained unchanged during an interval of 30 h at 453 K and 1 bar, suggesting that they were very promising for long-term operation.

4. Conclusions

In short, in this study, we successfully manufactured well-intergrown, highly *c*-oriented ultrathin 2D Cu-TCPP membranes by facile in-situ solvothermal growth. Among various synthetic parameters, substrate surface decoration with LDH-based ZnO buffer layers, employing $Cu(acac)_2$ as copper source, and addition of TEA as structural modulator during in-situ solvothermal growth were found to be essential for obtaining 2D Cu-TCPP membranes with the desired microstructure.

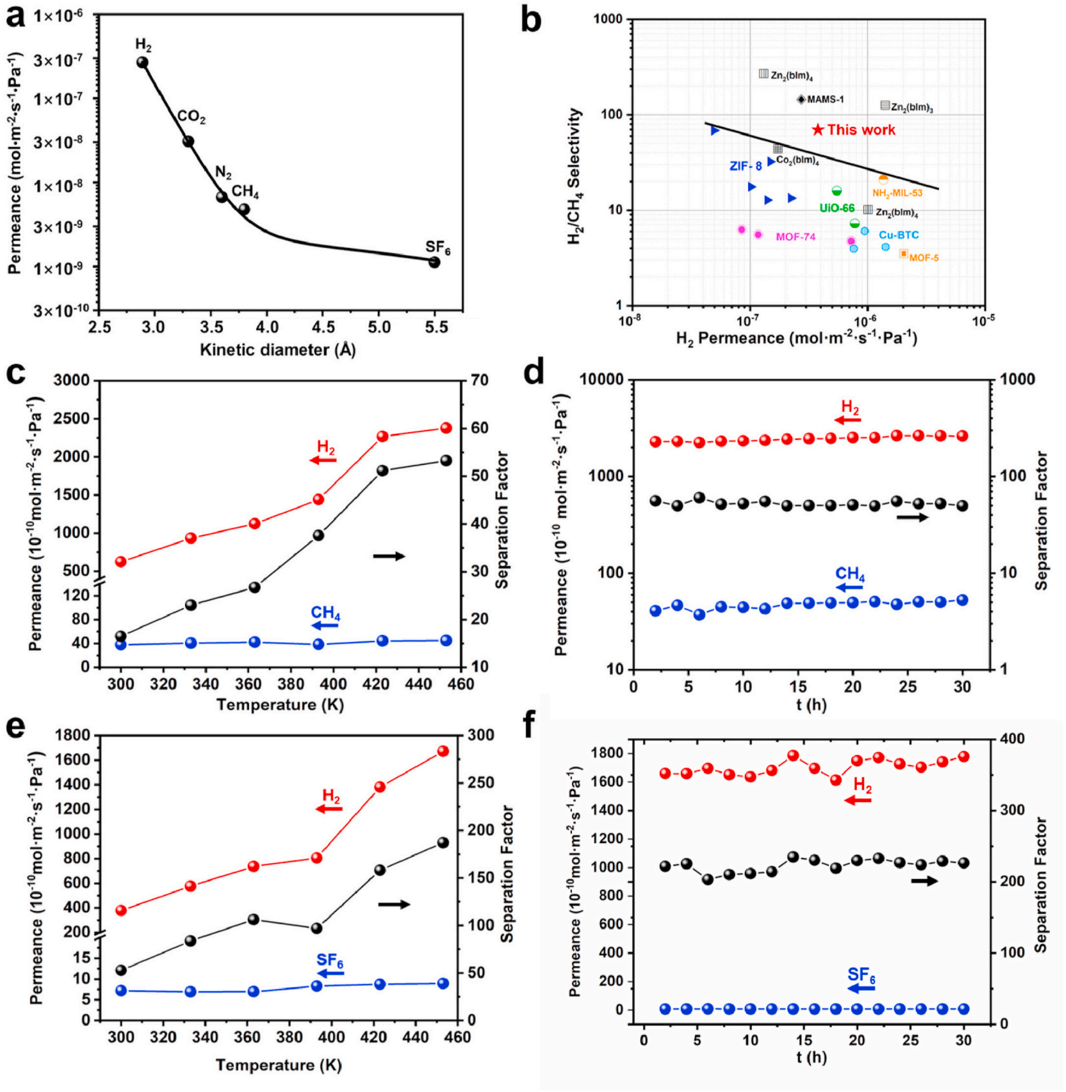

Fig. 4. (a) The permeance behavior of single gases through 2D Cu-TCPP membrane as a function of the kinetic diameter of gas molecules at 453 K and 1 bar. (b) H_2/CH_4 separation performance of 2D Cu-TCPP membrane in comparison with typical polycrystalline MOF membranes as reported in the literature (black line) such as MAMS-1 [8], [$Zn_2(bIm)_4$] [9,44], [$Zn_2(bIm)_3$] [10], [$Co_2(bIm)_4$] [43], Cu-BTC [40–42], UiO-66 [34,35], NH_2-MIL-53 [38], MOF-74 [14,39], MOF-5 [32] and ZIF-8 [17,18,33,36,37]. (c) Evaluation the H_2/CH_4 separation performance of 2D Cu-TCPP membrane on different operating temperatures ($\Delta P = 1$ bar). (d) Long-term operational stability of 2D Cu-TCPP membrane towards equimolar H_2/CH_4 at 453 K and 1 bar. (e) Evaluation the H_2/SF_6 separation performance of 2D Cu-TCPP membrane on different operating temperatures ($\Delta P = 1$ bar). (f) Long-term operational stability of 2D Cu-TCPP membrane towards equimolar H_2/SF_6 at 453 K and 1 bar.

Relying on the regular stacking between adjacent Cu-TCPP nanosheets, the equivalent in-plane pore size of 2D Cu-TCPP membranes reached ~5.4 Å, resulting in superb selectivity towards H_2/N_2, H_2/CH_4, and H_2/SF_6 gas pairs. Our research highlighted the importance of concurrent stacking mode utilization on a microscopic scale and microstructural optimization on a mesoscopic scale in preparing 2D membranes with precise size-selective molecular sieving ability.

Author statement

Yi Liu conceived the idea and designed the experiments. Yifan Song performed major experiments and analyzed the experimental data. Yanwei Sun helped with the synthesis of 2D Cu-TCPP membranes. Dongying Du helped draw the crystal structure of 2D Cu-TCPP with the Diamond software. Mu Zhang and Yi Liu helped with the gas permeation test. Liangliang Liu and Taotao Ji helped with relevant morphological characterization. Gaohong He assisted in analyzing the experimental data. Yi Liu and Yifan Song co-wrote the manuscript with contributions from all authors. We all authors guarantee that the above information is reliable and correct.

Declaration of competing interest

The authors declare that they have no known competing financial interests or personal relationships that could have appeared to influence the work reported in this paper.

Acknowledgements

This work was supported by Science Fund for Creative Research Groups of the National Natural Science Foundation of China (22021005), National Natural Science Foundation of China (22078039, 21176231), Fok Ying-Tong Education Foundation of China (171063), Liaoning Revitalization Talents Program (XLYC1807084), National Key Research and Development Program of China (2019YFE0119200), and the Technology Innovation Team of Dalian University of Technology

(DUT2017TB01).

Appendix A. Supplementary data

Supplementary data to this article can be found online at https://doi.org/10.1016/j.memsci.2021.119393.

References

[1] Y. Peng, Y.S. Li, Y.J. Ban, H. Jin, W.M. Jiao, X.L. Liu, W.S. Yang, Metal-organic framework nanosheets as building blocks for molecular sieving membranes, Science 346 (2014) 1356–1359, https://doi.org/10.1126/science.1254227.

[2] K. Varoon, Y. Zhang, B. Elyassi, D.D. Brewer, M. Gettel, S. Kumar, J.A. Lee, S. Maheshwari, A. Mittal, Y. Sung, M. Cococcioni, L.F. Francis, A.V. Mccormick, K. A. Mkhoyan, M. Tsapatsis, Dispersible exfoliated zeolite nanosheets and their application as a selective membrane, Science 334 (2011) 72–75, https://doi.org/10.1126/science.1208891.

[3] H.Y. Kim, H.W. Yoon, S.M. Yoon, B.M. Yoo, B.K. Ahn, Y.H. Cho, H.J. Shin, H. Yang, U. Paik, S. Kwon, J.Y. Choi, H.B. Park, Selective gas transport through few-layered graphene and graphene oxide membranes, Science 342 (2013) 91–95, https://doi.org/10.1126/science.1236098.

[4] D.K. Chen, W. Ying, Y. Guo, Y.L. Ying, X.S. Peng, Enhanced gas separation through nanoconfined ionic liquid in laminated MoS$_2$ membrane, ACS Appl. Mater. Interfaces 9 (2017) 44251–44257, https://doi.org/10.1021/acsami.7b15762.

[5] H.W. Fan, A. Mundstock, A. Feldhoff, A. Knebel, J.H. Gu, H. Meng, J. Caro, Covalent organic framework–covalent organic framework bilayer membranes for highly selective gas separation, J. Am. Chem. Soc. 140 (2018) 10094–10098, https://doi.org/10.1021/jacs.8b05136.

[6] Y. Li, Q.X. Wu, X.H. Guo, M.C. Zhang, B. Chen, G.Y. Wei, X. Li, X.F. Li, S.J. Li, L. J. Ma, Laminated self-standing covalent organic framework membrane with uniformly distributed subnanopores for ionic and molecular sieving, Nat. Commun. 11 (2020) 599–608, https://doi.org/10.1038/s41467-019-14056-7.

[7] J. Shen, G.Z. Liu, Y.F. Ji, Q. Liu, L. Cheng, K.C. Guan, M.C. Zhang, G.P. Liu, J. Xiong, J. Yang, W.Q. Jin, 2D MXene nanofilms with tunable gas transport channels, Adv. Funct. Mater. 28 (2018), 1801511, https://doi.org/10.1002/adfm.201801511.

[8] X.R. Wang, C.L. Chi, K. Zhang, Y.H. Qian, K.M. Gupta, Z.X. Kang, J.W. Jiang, D. Zhao, Reversed thermo-switchable molecular sieving membranes composed of two-dimensional metal-organic nanosheets for gas separation, Nat. Commun. 8 (2017), 14460, https://doi.org/10.1038/ncomms14460.

[9] Y.J. Li, H.O. Liu, H.T. Wang, J.S. Qiu, X.F. Zhang, GO-guided direct growth of highly oriented metal-organic framework nanosheet membranes for H$_2$/CO$_2$ separation, Chem. Sci. 9 (2018) 4132–4141, https://doi.org/10.1039/c7sc04815g.

[10] Y. Peng, Y.S. Li, Y.J. Ban, W.S. Yang, Two-dimensional metal-organic framework nanosheets for membrane-based gas separation, Angew. Chem. Int. Ed. 56 (2017) 9757–9761, https://doi.org/10.1002/anie.201703959.

[11] Z.W. Jiang, Y.C. Zou, T.T. Zhao, S.J. Zhen, Y.F. Li, C.Z. Huang, Controllable synthesis of porphyrin-based 2D lanthanide metal-organic frameworks with thickness- and metal-node-dependent photocatalytic performance, Angew. Chem. Int. Ed. 59 (2020) 3300–3306, https://doi.org/10.1002/ange.201913748.

[12] R. Makiura, S. Motoyama, Y. Umemura, H. Yamanaka, O. Sakata, H. Kitagawa, Surface nano-architecture of a metal-organic framework, Nat. Mater. 9 (2010) 565–571, https://doi.org/10.1038/NMAT2769.

[13] G. Xu, K. Otsubo, T. Yamada, S. Sakaida, H. Kitagawa, Superprotonic conductivity in a highly oriented crystalline metal-organic framework nanofilm, J. Am. Chem. Soc. 135 (2013) 7438–7441, https://doi.org/10.1021/ja402727d.

[14] N.Y. Wang, A. Mundstock, Y. Liu, A.S. Huang, J. Caro, Amine-modified Mg-MOF-74/CPO-27-Mg membrane with enhanced H$_2$/CO$_2$ separation, Chem. Eng. Sci. 124 (2015) 27–36, https://doi.org/10.1016/j.ces.2014.10.037.

[15] S. Motoyama, R. Makiura, O. Sakata, H. Kitagawa, Highly crystalline nanofilm by layering of porphyrin metal-organic framework sheets, J. Am. Chem. Soc. 133 (2011) 5640–5643, https://doi.org/10.1021/ja110720f.

[16] G. Xu, T. Yamada, K. Otsubo, S. Sakaida, H. Kitagawa, Facile "modular assembly" for fast construction of a highly oriented crystalline MOF nanofilm, J. Am. Chem. Soc. 134 (2012) 16524–16527, https://doi.org/10.1021/ja307953m.

[17] Y. Liu, J.H. Pan, N.Y. Wang, F. Steinbach, X.L. Liu, J. Caro, Remarkably enhanced gas separation by partial self-conversion of a laminated membrane to metal-organic frameworks, Angew. Chem. Int. Ed. 54 (2015) 3028–3032, https://doi.org/10.1002/anie.201411550.

[18] X.F. Zhang, Y.G. Liu, L.Y. Kong, H.O. Liu, J.S. Qiu, W. Han, L.-T. Weng, K.L. Yeung, W.D. Zhu, A simple and scalable Method for preparing low-defect ZIF-8 tubular membranes, J. Mater. Chem. A. 1 (2013) 10635–10638, https://doi.org/10.1039/c3ta12234d.

[19] X.F. Zhang, Y.G. Liu, S.H. Li, L.Y. Kong, H.O. Liu, Y.S. Li, W. Han, K.L. Yeung, W. D. Zhu, W.S. Yang, J.S. Qiu, New membrane architecture with high performance: ZIF-8 membrane supported on vertically aligned ZnO nanorods for gas permeation and separation, Chem. Mater. 26 (2014) 1975–1981, https://doi.org/10.1021/cm500269e.

[20] P. Nian, Y.J. Li, X. Zhang, Y. Cao, H.O. Liu, X.F. Zhang, ZnO nanorod-induced heteroepitaxial growth of SOD type Co-based zeolitic imidazolate framework membranes for H$_2$ separation, ACS Appl. Mater. Interfaces 10 (2018) 4151–4160, https://doi.org/10.1021/acsami.7b17568.

[21] L.Y. Kong, X.F. Zhang, H.O. Liu, J.S. Qiu, Synthesis of a highly stable ZIF-8 membrane on a macroporous ceramic tube by manual-rubbing ZnO deposition as a multifunctional layer, J. Membr. Sci. 490 (2015) 354–363, https://doi.org/10.1016/j.memsci.2015.05.006.

[22] K. Khaletskaya, S. Turner, M. Tu, S. Wannapaiboon, A. Schneemann, R. Meyer, A. Ludwig, G. Van Tendeloo, R.A. Fischer, Self-directed localization of ZIF-8 thin film formation by conversion of ZnO nanolayers, Adv. Funct. Mater. 24 (2014) 4804–4811, https://doi.org/10.1002/adfm.201400559.

[23] Y. Liu, Y. Peng, N.Y. Wang, Y.S. Li, J.H. Pan, W.S. Yang, J. Caro, Significantly enhanced separation using ZIF-8 membranes by partial conversion of calcined layered double hydroxide precursors, ChemSusChem 8 (2015) 3582–3586, https://doi.org/10.1002/cssc.201500977.

[24] D.T. Lee, J.D. Jamir, G.W. Peterson, G.N. Parsons, Water-stable chemical-protective textiles via euhedral surface-oriented 2D Cu-TCPP metal-organic frameworks, Small 15 (2019), 1805133, https://doi.org/10.1002/smll.201805133.

[25] Y.W. Sun, S. Hu, C.S. Song, S. Miao, Z. Jiang, X. Jiang, J.J. Zhao, X.W. Guo, Y. Liu, Two-dimensional transition metal dichalcogenides as metal sources of metal-organic frameworks, Chem. Commun. 54 (2018) 3664–3667, https://doi.org/10.1039/c8cc01258j.

[26] Y.W. Sun, Y. Liu, J. Caro, X.W. Guo, C.S. Song, Y. Liu, In-plane epitaxial growth of highly c-oriented NH$_2$ -MIL-125(Ti) membranes with superior H$_2$/CO$_2$ selectivity, Angew. Chem. Int. Ed. 57 (2018) 16088–16093, https://doi.org/10.1002/anie.201810088.

[27] Y. Sun, C. Song, X. Guo, Y. Liu, Concurrent manipulation of out-of-plane and regional in-plane orientations of NH$_2$-UiO-66 membranes with significantly reduced anisotropic grain boundary and superior H$_2$/CO$_2$ separation performance, ACS Appl. Mater. Interfaces 12 (2020) 4494–4500, https://doi.org/10.1021/acsami.9b18804.

[28] Y.J. Li, L. Lin, M. Tu, P. Nian, A.J. Howarth, O.K. Farha, J.S. Qiu, X.F. Zhang, Growth of ZnO self-converted 2D nanosheet zeolitic imidazolate framework membranes by an ammonia- assisted strategy, Nano Res 11 (2018) 1850–1860, https://doi.org/10.1007/s12274-017-1803-0.

[29] D.D. La, H.P.N. Thi, Y.S. Kim, A. Rananaware, S.V. Bhosale, Facile fabrication of Cu (II)-porphyrin MOF thin films from tetrakis(4-carboxyphenyl)porphyrin and Cu (OH)$_2$ nanoneedle array, Appl. Surf. Sci. 424 (2017) 145–150, https://doi.org/10.1016/j.apsusc.2017.01.110.

[30] M. Zhou, J. Hedlund, Facile preparation of hydrophobic colloidal MFI and CHA crystals and oriented ultrathin films, Angew. Chem. Int. Ed. 57 (2018) 10966–10970, https://doi.org/10.1002/ange.201806502.

[31] Z.X. Zhao, X.L. Ma, Z. Li, Y.S. Lin, Synthesis, characterization and gas transport properties of MOF-5 membranes, J. Membr. Sci. 382 (2011) 82–90, https://doi.org/10.1016/j.memsci.2011.07.048.

[32] Y.Y. Liu, Z.F. Ng, E.A. Khan, H.-K. Jeong, C.-b. Ching, Z.P. Lai, Synthesis of continuous MOF-5 membranes on porous α-alumina substrates, Microporous Mesoporous Mater. 118 (2009) 296–301, https://doi.org/10.1016/j.micromeso.2008.08.054.

[33] H. Bux, A. Feldhoff, J. Cravillon, M. Wiebcke, Y.-S. Li, J. Caro, Oriented zeolitic imidazolate framework-8 membrane with sharp H$_2$/C$_3$H$_8$ molecular sieve separation, Chem. Mater. 23 (2011) 2262–2269, https://doi.org/10.1021/cm200555s.

[34] S. Friebe, B. Geppert, F. Steinbach, J. Caro, Metal-organic framework UiO-66 layer: a highly oriented membrane with good selectivity and hydrogen permeance, ACS Appl. Mater. Interfaces 9 (2017) 12878–12885, https://doi.org/10.1021/acsami.7b02105.

[35] X.L. Liu, N.K. Demir, Z.T. Wu, K. Li, Highly water-stable zirconium metal-organic framework UiO-66 membranes supported on alumina hollow fibers for desalination, J. Am. Chem. Soc. 137 (2015) 6999–7002, https://doi.org/10.1021/jacs.5b02276.

[36] Q. Liu, N.Y. Wang, J. Caro, A.S. Huang, Bio-inspired polydopamine: a versatile and powerful platform for covalent synthesis of molecular sieve membranes, J. Am. Chem. Soc. 135 (2013) 17679–17682, https://doi.org/10.1021/ja4080562.

[37] Y. Liu, N.Y. Wang, J.H. Pan, F. Steinbach, J. Caro, In situ synthesis of MOF membranes on ZnAl-CO$_3$ LDH buffer layer-modified substrates, J. Am. Chem. Soc. 136 (2014) 14353–14356, https://doi.org/10.1021/ja507408s.

[38] F. Zhang, X.Q. Zou, X. Gao, S.J. Fan, F.X. Sun, H. Ren, G.S. Zhu, Hydrogen selective NH$_2$-MIL-53(Al) MOF membranes with high permeability, Adv. Funct. Mater. 22 (2012) 3583–3590, https://doi.org/10.1002/adfm.201200084.

[39] X. Qin, Y.X. Sun, N.X. Wang, Q. Wei, L.H. Xie, Y.B. Xie, J.-R. Li, Nanostructure array assisted aggregation-based growth of a Co-MOF-74 membrane on a Ni-foam substrate for gas separation, RSC Adv. 6 (2016) 94177–94183, https://doi.org/10.1039/c6ra21320k.

[40] H.L. Guo, G.S. Zhu, L.J. Hewitt, S.L. Qiu, “Twin copper source” growth of metal-organic framework membrane: Cu$_3$(BTC)$_2$ with high permeability and selectivity for recycling H$_2$, J. Am. Chem. Soc. 131 (2009) 1646–1647, https://doi.org/10.1021/ja8074874.

[41] V.V. Guerrero, Y. Yoo, M.C. McCarthy, H.-K. Jeong, HKUST-1 membranes on porous supports using secondary growth, J. Mater. Chem. 20 (2010) 3938–3943, https://doi.org/10.1039/b924536g.

[42] J.P. Nan, X.L. Dong, W.J. Wang, W.Q. Jin, N.P. Xu, Step by-step seeding procedure for preparing HKUST-1 membrane on porous α-alumina support, Langmuir 27 (2011) 4309–4312, https://doi.org/10.1021/la200103w.

[43] P. Nian, H.O. Liu, X.F. Zhang, Bottom-up fabrication of two-dimensional Co-based zeolite imidazolate framework tubular membranes consisting of nanosheets by vapor phase transformation of Co-based gel for H$_2$/CO$_2$ separation, J. Membr. Sci. 573 (2019) 200–209, https://doi.org/10.1016/j.memsci.2018.11.076.

[44] K. Yang, Y.J. Ban, A. Guo, M. Zhao, Y.W. Zhou, N. Cao, W.S. Yang, In-situ interfacial assembly of ultra-H_2-permeable metal-organic framework membranes for H_2/CO_2 separation, J. Membr. Sci. 611 (2020), 118419, https://doi.org/10.1016/j.memsci.2020.118419.

[45] R. Krishna, J.M. Baten, Maxwell-Stefan modeling of slowing-down effects in mixed gas permeation across porous membranes, J. Membr. Sci. 383 (2011) 289–300, https://doi.org/10.1016/j.memsci.2011.08.067.

[46] R. Rong, Y.W. Sun, T.T. Ji, Y. Liu, Fabrication of highly CO_2/N_2 selective polycrystalline UiO-66 membrane with two-dimensional transition metal dichalcogenides as zirconium source via tertiary solvothermal growth, J. Membr. Sci. 610 (2020), 118275, https://doi.org/10.1016/j.memsci.2020.118275.

[47] M. Miyamoto, K. Hori, T. Goshima, N. Takaya, Y. Oumi, S. Uemiya, An organoselective Zirconium-based metal-organic framework UiO-66 membrane for pervaporation, Eur. J. Inorg. Chem. 14 (2017) 2094–2099, https://doi.org/10.1002/ejic.201700010.

[48] C. Chmelik, H. Voss, H. Bux, J. Caro, Adsorption and diffusion-basis for molecular understanding permeation through molecular sieve membranes, Chem. Ing. Tech. 83 (2011) 104–112, https://doi.org/10.1002/cite.201000179.